Geophysical Journal International

Geophys. J. Int. (2012) **189,** 863–876 doi: 10.1111/j.1365-246X.2012.05401.x

Consistent patterns of Antarctic ice sheet interannual variations from ENVISAT radar altimetry and GRACE satellite gravimetry

Martin Horwath,[1,2,★] Benoît Legrésy,[1] Frédérique Rémy,[1] Fabien Blarel[1] and Jean-Michel Lemoine[2]

[1]*LEGOS,* 18, *av. E. Belin,* 31401 *Toulouse Cedex* 9, *France. E-mail: martin.horwath@legos.obs-mip.fr, martin.horwath@bv.tum.de*
[2]*CNES/GRGS,* 18, *av. E. Belin,* 31401 *Toulouse Cedex* 9, *France*

Accepted 2012 January 29. Received 2011 December 21; in original form 2010 October 21

SUMMARY

Interannual variations of the Antarctic ice sheet due to surface mass balance (SMB) fluctuations are important for mass balance estimates and interpretations. To date, these variations are primarily assessed by global or regional atmospheric modelling. Satellite altimetry and satellite gravimetry over the ice sheet provide complementary observations of the related volume and mass effects, respectively. Yet, so far the interannual signal contents of these observations have not been extensively studied. We compare and jointly interpret ENVISAT radar altimetry (RA) and GRACE satellite gravimetry results, relying on RA products from the along-track repeat satellite RA approach and on the GRACE 10-d solutions by CNES/GRGS. RA results and GRACE results are expressed in terms of variations of ice sheet thickness, $\Delta z(t)$, and ice-equivalent thickness, $\Delta z_{\rm ice}(t)$, respectively. In view of the different errors and limitations of both techniques and of differences between $\Delta z(t)$ and $\Delta z_{\rm ice}(t)$ expected due to firn-related processes, our principal approach is a comparison of qualitative patterns in space and time. To adjust the spatial resolution of both data sets, we describe the spatial filtering inherent to the regularization of the CNES/GRGS GRACE solutions and apply this filtering to the ENVISAT RA height changes in a consistent fashion. After correction for glacial isostatic adjustment, the spatial patterns of linear trends seen by ENVISAT RA and GRACE over the period 2002 October to 2009 August agree well, not only for the extreme ice losses in the West Antarctic Amundsen Sea Sector but also for an alternating sequence of gains and losses along the East Antarctic coast. Our main focus is on interannual signals, which we represent by the low-pass filtered non-linear, non-seasonal components of the $\Delta z(t)$ and $\Delta z_{\rm ice}(t)$ time-series. These components should reflect interannual SMB variations, apart from effects of changes in ice flow. We find an agreement between the interannual variation patterns from ENVISAT RA and GRACE with temporal correlation coefficients typically in the order of 0.8. This qualitative agreement, prevailing even in the theoretical absence of a simple proportionality between $\Delta z(t)$ and $\Delta z_{\rm ice}(t)$, indicates that both observational signals primarily originate in common geophysical variations. Combining both geodetic data sets aids their interpretation and promises to be valuable for the reduction of SMB uncertainties. In a case study based on the analysis of both GRACE and ENVISAT RA, we identify a prominent interannual feature in West Antarctica in 2005 September/October as an event of excess snow accumulation with a mass effect of 82 ± 31 Gt.

Key words: Satellite geodesy; Sea level change; Time variable gravity; Global change from geodesy; Glaciology; Antarctica.

1 INTRODUCTION

Reactions of the Antarctic ice sheet to changes of its atmospheric, oceanic and solid Earth boundary conditions occur at timescales from millennia to hours (Alley *et al.* 2005; Bindschadler 2006). While most researchers agree that in the last decade ice mass changes have been dominated by losses due to accelerated outflow in West Antarctica, predictions for the next century are uncertain, even in sign (Solomon *et al.* 2007).

The mass balance of the grounded ice sheet is the difference between mass input by net snow accumulation (surface mass balance,

★Now at: Institut für Astronomische und Physikalische Geodäsie, Technische Universität München, Arcisstr. 21, D-80333 München, Germany.

SMB) and mass output by ice flux across the grounding line. Outflux is commonly deduced from satellite observations of surface flow velocities (Rignot *et al.* 2008). SMB data are obtained from sparse *in situ* observations, remote sensing and atmospheric modelling (Vaughan *et al.* 1999; Greuell & Genthon 2004; van de Berg *et al.* 2006; Eisen *et al.* 2008; Monaghan & Bromwich 2008) where recent mass balance-oriented estimates (Rignot *et al.* 2008, 2011) resort to modelling validated by observations.

Despite great progress in recent years (e.g. van den Broeke *et al.* 2011), uncertainties of the SMB and its interannual variations remain a major limitation for mass balance estimates from calculating the difference between SMB and ice outflux (van den Broeke *et al.* 2011; Rignot *et al.* 2011). More observational data could improve quantifications of the actual SMB and, moreover, help to validate and improve the representation of SMB-related processes in atmospheric models.

There are two approaches of observing changes on an ice sheet scale by satellite geodesy. The first one is to observe surface height variations, which may be converted to mass variations under additional assumptions. Since 1991, satellite radar altimetry (RA) has enabled this approach (Davis *et al.* 2005; Zwally *et al.* 2005; Wingham *et al.* 2006) with the sequence of the ERS-1, ERS-2 and ENVISAT missions, recently supplemented by CryoSat-2. As one of its problems, RA has had limitations of coverage at the ice sheet margins and in the polar gap beyond 81.5° latitude. A second limitation arises from the complexity of radar reflections at an ice sheet, including time-variable penetration effects (Legrésy & Rémy 1997, 1998; Arthern *et al.* 2002). In this context, Thomas *et al.* (2008) challenged the origin of altimetric height trends over the interior of Greenland. Satellite laser altimetry as realized by the ICESat mission (2002–2009; Schutz *et al.* 2005; Pritchard *et al.* 2009) has no problem of signal penetration and of signal loss at ice sheet margins. However, the achieved temporal sampling (2–3 months per year) degrades the quality of studies of linear trends (Gunter *et al.* 2009) and tends to undermine studies of non-linear interannual and seasonal variations.

The second geodetic approach is to observe the effect of mass redistributions on the Earth's gravity field. This has been realized since 2002 with the Gravity Recovery and Climate Experiment (GRACE) mission (Ramillien *et al.* 2006; Chen *et al.* 2008; Velicogna 2009; Horwath & Dietrich 2009; Sasgen *et al.* 2010b). Major limitations are the insensitivity of GRACE to spatial scales below a few hundred kilometres and the problem of separating linear ice mass changes from solid Earth mass displacements due to glacial isostatic adjustment (GIA).

Due to their different sensitivities, error sources and limitations, the different approaches have delivered a wide range of results about changes of the Antarctic ice sheet (Alley *et al.* 2007; Allison *et al.* 2009). Even results from the same satellite data and for similar time intervals may differ considerably depending on data analysis details [see, e.g. Alley *et al.* (2007) for RA and Sasgen *et al.* (2007) and Horwath & Dietrich (2009) for GRACE]. A comparison and, more rigorously, a combination of different techniques (e.g. Arthern & Hindmarsh 2003) is the way to gain understanding about their underlying geophysical processes and errors and to reduce the ambiguities inherent to any single technique. James & Ivins (1995) anticipated the combination of GPS, satellite gravity data and polar motion observations to constrain Antarctic ice mass changes. Regarding the combination of GRACE and satellite altimetry, a methodological foundation was laid by Wahr *et al.* (2000). Such a combination has to account for, and may exploit, the different relative sensitivities of satellite gravimetry and altimetry to ice sheet changes and GIA and the sensitivity of altimetry (but insensitivity of GRACE) to changes in the firn density structure (see Section 2.6). As a first practical realization, Gunter *et al.* (2009) and Riva *et al.* (2009) compared and combined linear trends from GRACE and ICESat laser altimetry.

Most GRACE or altimetry studies over ice sheets have followed the paradigm of long-term linear, or possibly quadratic, trends. In this context, interannual effects, notably those induced by SMB variations, appear as noise, which masks the long-term evolution and complicates the interpretation of trends over a few years (Rémy & Parrenin 2004). Recent RA analyses (Zwally *et al.* 2005; Helsen *et al.* 2008) employ models to assess how the observed trends are affected by interannual fluctuations of SMB and firn compaction, but they do not compare the modelled and observed non-linear fluctuations over the RA period. From a different point of view, reliable geodetic data on interannual variations could be valuable for time-variable SMB studies.

GRACE results over Antarctica show significant interannual variations beyond a linear or quadratic trend. An example is a positive anomaly that started in the second half of 2005 (Horwath & Dietrich 2009, fig. 15 and Velicogna 2009, fig. 2). Part of this interannual variability has been related to SMB (Sasgen *et al.* 2010a) but other features could arise from temporally correlated errors in the underlying GRACE solutions (Horwath & Dietrich 2009; Horwath *et al.* 2011). Sometimes, the geographic patterns aid a common-sense distinction between signals and artefacts (Horwath & Dietrich 2006), but the low spatial resolution of GRACE results limits this approach.

In this paper we explore the combination of GRACE and concurrent ENVISAT RA. Despite their limitations, the RA data have their unique advantages: The continuity of observation over two decades provides the longer-term context of more recent observations. By the temporal sampling along a 35-d repeat orbit, ENVISAT RA is the natural geometric complement to GRACE for jointly resolving the seasonal, interannual and long-term components of geographically dependent volume and mass changes, respectively. Here we focus on the interannual components which are expected to contain SMB-related signals.

In Section 2 we introduce the used data products and explain our approach of analysis. This approach accounts for the different spatial resolutions of the used ENVISAT RA and GRACE data products and for our limited knowledge of their error content, particularly concerning interannual variations, which have been less studied than trends and which are observed with less redundancy. It cannot be taken for granted from the start that the interannual variations in ENVISAT RA and GRACE reliably reflect geophysical signals and are useful for a synthesis of both techniques. From this starting point, our principal approach will be to assess the qualitative consistency between patterns of ENVISAT RA and GRACE results. As explicated in Section 2.6, these patterns are expressed in terms of ice sheet thickness variations $\Delta z(t)$ and ice-equivalent thickness variations $\Delta z_{\mathrm{ice}}(t)$, respectively, for ENVISAT RA and GRACE. Even though no simple proportionality between $\Delta z(t)$ and $\Delta z_{\mathrm{ice}}(t)$ can be expected, qualitative agreement between ENVISAT RA and GRACE patterns would indicate that both techniques are mature enough to primarily reflect true geophysical signals. In Section 3 we present our results, which indeed show consistency between the GRACE and ENVISAT RA patterns of both linear and interannual variations. We then further explore and discuss the synthesis of both techniques. Finally, Section 4 draws the conclusions.

2 DATA AND METHODS

2.1 ENVISAT RA

Like its altimetric predecessors ERS-1 and ERS-2, ENVISAT carries a Ku-Band (13.6 GHz) radar altimeter on a sun-synchronous 35-d repeat orbit with a 98.5° inclination (ESA 2007). The ENVISAT Ice-2 waveform retracker (Legrésy *et al.* 2005; ESA 2007) provides the altimetric range together with three other waveform parameters (leading edge width, trailing edge slope and backscattering coefficient). We apply the corrections for Earth tides and pole tides, tidal loading (from the ENVISAT geophysical data records; ESA 2007), and for ionospheric delay [GIM model (Iijima *et al.* 1999)]. We do not apply tropospheric refraction corrections because they are subject to caution over ice sheets (Blarel 2010). Tropospheric correction time-series generated from ERA interim data (Berrisford *et al.* 2009) mainly exhibit a seasonal behaviour while their interannual signal is negligible in comparison with other interannual signals in the height data.

Following the along-track repeat satellite RA approach (Legrésy *et al.* 2006), 35-daily time-series of altimetric parameters are analysed every 370 m along the repeat tracks. The altimetric parameters are corrected for differential topographic effects between the individual measurements due to the non-exact repeat of the observation positions and the small-scale topography (geographic correction). Within every 370 m × 2 km box (along-track sampling distance × cross-track repeat band) the topographic effect is modelled as a function of the position, which is adjusted and removed (Legrésy *et al.* 2006).

The radar response comprises a surface echo and a volume echo (Legrésy & Rémy 1997, 1998; Arthern *et al.* 2002). Their shapes and relative proportions change when properties of the snow surface and the upper firn layers change. Such changes may induce artificial height changes for any retracking procedure (Legrésy & Rémy 1998). Our empirical approach to correct for such artefacts is based on the assumption that a change in surface or firn characteristics will also change at least one of the other three waveform parameters. We assume a linear relation between changes in the three waveform parameters and related height artefacts. For every 370 m along-track bin we determine the respective linear regression and subsequently reduce those height change components that are linearly related to changes in the waveform parameters (Legrésy *et al.* 2006).

Legrésy *et al.* (2006) demonstrated how the geographic and echo shape correction largely reduce the variability of the original altimetric height time-series. Lacroix *et al.* (2009) investigated the altimetric signature of a meteorological event that changed surface properties in the Lake Vostok region in interior East Antarctica. The effect on the raw altimetric height was a jump of 41 cm. This obvious artefact was reduced to 1 cm by the waveform shape correction. In contrast, a jump of 6 cm remained when the authors employed an empirical correction (Wingham *et al.* 1998; Zwally *et al.* 2005) solely based on backscatter variations. Nonetheless, also with the advanced correction, some unknown residual time-variable penetration effects have to be expected in our RA products.

For subsequent analyses the along-track time-series with at least 30 repeat observations are condensed to a time-series of grids with a longitude/latitude spacing of 0.75° × 0.2°. We choose overlapping 35-d intervals every 10 d such that their centres correspond to the centres of the GRACE 10-d solution intervals (Section 2.2). For each 35-d interval, each grid cell with at least 10 observations over grounded ice is assigned with the average of those observations.

For every grid cell, the mean value is subtracted from the time-series, and an outlier elimination is performed. Grid cell time-series with less than 200 values or less than 5 yr length are completely rejected. Finally, the sampling is reduced to the times where both ENVISAT RA and GRACE data (see next section) are available, that is, to the epochs from 2002 October 22 to 2009 August 26 with 16 epochs missing. To calculate ENVISAT RA volume changes over an Antarctic basin, we sum up the height variations per grid cell multiplied with the cell area, ignoring cells with no data.

The results are obviously subject to the limitations of ENVISAT RA coverage. The polar gap beyond 81.5° latitude is not covered and in steep coastal regions, abrupt transitions and heavily crevassed areas, conventional pulse-limited RA fails to properly track the radar echo. In addition, the results may be affected by ENVISAT RA sampling properties since the ENVISAT RA observations actually refer to the surface patch with smallest distance to the satellite which may be several kilometres upslope from the nadir point (Rémy *et al.* 1989) deforming the tracks to an irregular sampling (Roemer *et al.* 2007). In case of small-scale dynamic changes in rugged terrain this may be an issue for the representativeness of the ENVISAT RA sampling (Thomas *et al.* 2008). One could choose sophisticated approaches to account for the ENVISAT RA sampling characteristics and to interpolate or extrapolate to uncovered areas, based on additional modelling choices. In this study, however, we restrict ourselves to the information that may be directly deduced from the RA observations.

2.2 GRACE satellite gravimetry

The GRACE mission launched in 2002 (Schmidt *et al.* 2008) senses temporal changes of the Earth's gravity field through their orbital effects measured in a differential manner by a microwave ranging system between the two coorbiting satellites. Temporal gravity field changes may then be translated into geographically dependent equivalent surface mass changes (Wahr *et al.* 1998), expressed in terms of water equivalent (w.e.) or ice equivalent height. We will employ ice equivalent height variations Δz_{ice}.

Here we use the CNES/GRGS time-variable gravity field solutions of Release 2 produced from GRACE Level-1B data complemented by LAGEOS satellite laser ranging data (Lemoine *et al.* 2007; Bruinsma *et al.* 2010). The solutions are given in a spherical harmonic representation. Tidal and non-tidal atmospheric and oceanic mass variations are included in the background model of the gravity field estimation procedure and are not included in the time-variable solutions.

Release-2 (Bruinsma *et al.* 2010) comprises the mean model EIGEN-GRGS.RL02.mean-field (up to spherical harmonic degree 160) and a series of 10-d solutions (up to degree 50). The mean model was estimated from 4.5 yr of data (2003 February 27–2007 September 30) and includes some components of temporal changes, namely linear trends and annual and semi-annual sinusoidal components up to degree 50 and an additional jump associated to the 2005 December Sumatra earthquake. The 10-d solutions are regularized towards the mean model by applying tailored degree- and order-dependent constraints in the process of gravity field estimation. The regularization is a compromise between the suppression of noise and the preservation of geophysical signal. For unregularized solutions, in contrast, noise is usually attenuated by post-processing filters (e.g. Werth *et al.* 2009). Both regularization and post-processing filters affect, and potentially distort, geophysical

signal patterns. Bruinsma *et al.* (2010) analyse the regularization effect for the CNES/GRGS Release-2 solutions and compare them to filtered solutions by other GRACE processing institutions. For more investigations and comparisons of regularization and filtering effects, apart from the illustration given later, the reader is referred to, for example, Kusche (2007) and Werth *et al.* (2009).

In fact, the manner in which the CNES/GRGS regularization affects geophysical signals can be also interpreted as a filter. If the normal equation matrices of an unregularized solution and of a regularized solution (N_u and N_r) are available, this filter can be described by the fully populated filter matrix (Kusche 2007)

$$F = N_r^{-1} N_u. \quad (1)$$

A more detailed formal description of the filter effect on geophysical surface mass signals is provided in the Appendix. Following this approach of filter description we use normal equation matrices of the CNES/GRGS gravity field solutions to describe the filtering of geophysical signals inherent to the 10-d solutions. Note that the regularization of the 10-d solutions concerns only the differences with respect to the mean model. For example, the trend of the 10-d solutions, to the extent to which it is contained in the mean model, is not affected by this regularization. The trend of the mean model, for its part, was regularized with relatively weak constraints enabled by the long observation period. Hence, the filtering inherent to the trends in the series of 10-d solutions is different from the filtering inherent to the contained non-linear, non-seasonal anomalies. An analogous statement holds for the annual and semi-annual components.

Fig. 1 shows the filter response computed for synthetic mass signals concentrated at Pine Island Glacier in West Antarctica. Filter effects on a linear trend (subplot a) and on a non-linear, non-seasonal anomaly with respect to the 4.5-yr-mean linear and seasonal behaviour (subplot b) are shown. Both subplots illustrate the limited spatial resolution provided by the 10-d solutions. Already by the spectral truncation at degree 50, resolution is limited to 400 km half wavelength, and it is further reduced by the filtering inherent to the regularization. This filtering is non-isotropic. It further depends on the nature of the temporal signal (compare subplots a and b) and on latitude.

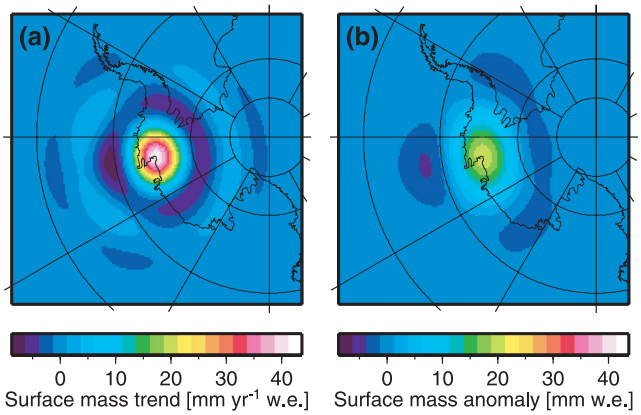

Figure 1. Effect of the filtering inherent to the CNES/GRGS 10-day GRACE solutions. The effect is simulated for two synthetic mass signals (discs of 25 km diameter) concentrated at the Pine Island Glacier terminus. (a) A linear trend of 10 Gt yr^{-1}; (b) a 10 Gt anomaly with respect to the linear and seasonal behaviour described by the EIGEN-GRGS.RL02.mean-field model. As explicated in the main text (Section 2.2, third and fourth paragraph), the effect on the two kinds of temporal signals is different because their degree of regularization is different.

To converge the temporal resolution of our GRACE time-series to that of the ENVISAT RA data representing 35-d averages, we average triples of GRACE 10-d solutions, thus generating a 10-daily time-series of overlapping 30-d averages. As for the ENVISAT RA time-series (see Section 2.1), the sampling is reduced to the epochs common to ENVISAT RA and GRACE.

For calculating integrated mass changes over subregions of the Antarctic ice sheet we adopt the methodology of Horwath & Dietrich (2009, their Method II) to the regularized but otherwise unfiltered GRACE time-variable solutions. In particular, the GRACE surface mass changes are integrated with a weight function that gently decreases from 1 to 0 within 400 km in oceans or ice shelves next to the region of interest.

Recognized error sources in the GRACE solutions, notably of errors that are correlated in time, are systematic errors in the intersatellite pointing data (Horwath *et al.* 2011), errors of the atmospheric mass variation models entering the background fields (Velicogna & Wahr 2010), and tidal aliasing (e.g. Moore & King 2008). For the case of regularized GRACE solutions, the filtering effect of the regularization changes with time, since in periods with reduced gravity field sensitivity of GRACE, for example, due to repeat orbit patterns (Klokočník *et al.* 2008), the solutions are tied more tightly to the reference solution than in other periods. The resulting heterogeneous representation of actual temporal variations has to be regarded as a part of the error budget.

2.3 GRACE-like filtering of ENVISAT RA

Surface mass variations from GRACE have much lower spatial resolution than height variations from ENVISAT RA. Our approach of comparing spatial patterns from both techniques is to filter the ENVISAT RA grids by a tailored filter (GRACE-like filter) that mimics the filtering inherent to the CNES/GRGS GRACE processing. In this way we produce maps of altimetric height variation patterns, effectively 'blurred' to the same extent as the GRACE images.

Based on the filter description in Section 2.2 we implemented the following algorithm for the GRACE-like filtering: (1) Transfer the altimetric height variations into the spherical harmonic domain. (Positions without valid value are set to zero.) (2) Decompose the temporal variations into a linear component, annual and semi-annual sinusoidal components and the remaining anomalies. To be consistent with the GRACE processing, the linear and sinusoidal parts are determined from only the 4.5 yr (2003 February–2007 July) that underlie the EIGEN-GRGS.RL02.mean-field model. (3) Filter the 10-daily data sets associated to the different temporal components using filter matrices (eq. 1) that correspond to the regularization of the respective components. Regarding the non-linear, non-seasonal components, a unique filter matrix (corresponding to a typical 10-d interval) is used for all 10-d intervals. Add up the filtered components. (4) Transfer the results into the spatial domain.

Note that in the subsequent analyses, whenever we consider trends or annual/semi-annual components of time-series, we adjust them to the full-length time-series.

2.4 GIA correction

We correct linear trends from ENVISAT RA and GRACE for the solid Earth's GIA to past ice load changes. The used model is based on the ice load history of Ivins & James (2005) and a mean mantle viscosity profile (see Horwath 2007, fig. 2.6 therein, for model maps). This state-of-the-art model, which is one of the GIA models

showing smallest disagreement to geodetic data (Riva *et al.* 2009; Thomas *et al.* 2011) was chosen to reduce, though not to completely eliminate, the GIA contamination of ice-sheet-related results (see further discussion in Section 2.6). We subject the GIA correction to the GRACE-like filtering when applying it to GRACE-like filtered ENVISAT RA maps or to GRACE maps.

The instantaneous elastic load response to ongoing surface mass changes is accounted for when converting GRACE gravity field changes to surface mass changes (Wahr *et al.* 1998), but is not accounted for in the ENVISAT RA analysis. The neglected effect is in the order of −2 per cent of the ice thickness change (Horwath 2007).

2.5 Considered temporal components

Changes of the ice sheet volume and mass include long-term, interannual, seasonal and intraannual components. This study concentrates on the interannual part which is derived based on a time-series decomposition into the linear, the seasonal and the remaining non-linear, non-seasonal component by simultaneously adjusting a constant, a trend and annual and semi-annual sinusoids. Our simple representation of interannual variations is then derived by low-pass filtering the residuals of the fit (i.e. the non-linear, non-seasonal components) with a Gaussian filter in the time domain (two-sigma width 0.5 yr, effecting a 50 per cent amplitude damping at 1.33 yr wavelength).

This representation of interannual variations is imperfect due to the difficulty of discriminating long-term and interannual components based on time-series of less than 7 yr. For example, interannual variability may induce a linear component of change, but we reduce those components. Conversely, in the case of an ongoing long-term linear acceleration of ice flow, long-term ice mass trends have a quadratic component (Velicogna 2009; Rignot *et al.* 2011), and this component remains included in our representation of interannual variations. We could choose to reduce quadratic components together with linear components but in this way we would inevitably absorb more truly interannual signal. In this context, Rignot *et al.* (2011), based on results of GRACE and of the mass budget method, have stated that 'an observation period of 8 yr is probably not sufficient for these methods to separate the long-term trend in ice sheet acceleration from temporal variations in SMB, especially in Antarctica'.

2.6 Preliminary considerations on comparing ENVISAT RA with GRACE

Changes of the ice sheet occur due to rapidly evolving ice flow dynamics and due to variations of SMB. Roughly speaking, in the first case the ratio between mass and volume change is the density of pure ice, while in the second case this ratio is the density of snow or firn, depending on the temporal scale of the changes. For a more general treatment, the ice sheet can be regarded as a mixture of pure ice and air, where the air is concentrated in the firn layer. Accordingly, the ice sheet thickness z is the sum of the equivalent thickness of pure ice z_{ice} and the equivalent thickness of a contained air layer z_{air}. The latter (sometimes called firn correction) is in the range from 0 to 44 m (Horwath *et al.* 2006; Ligtenberg *et al.* 2011). Ice flow, by concerning the entire vertical column, primarily affects z_{ice}. Snow accumulation increases both z_{ice} and z_{air}, and snow ablation decreases both. Compaction only reduces z_{air}.

In this context, the decomposition of ice sheet thickness changes Δz as a sum of changes in the equivalent ice and air layer thicknesses,

$$\Delta z = \Delta z_{\mathrm{ice}} + \Delta z_{\mathrm{air}}, \tag{2}$$

is a useful approach complementary to the consideration of the quotient between mass and volume change, $\rho_{\mathrm{ice}}\Delta z_{\mathrm{ice}}/\Delta z$ (where ρ_{ice} denotes the pure ice density). Indeed, if different processes are superimposed, the latter quotient may amount to any value between plus and minus infinity and cannot be simply associated with the density of a material added or removed. For an illustration, consider the superposition of an effect of rapidly evolving ice dynamics with $\Delta z_{\mathrm{ice}} = -0.3$ m, $\Delta z_{\mathrm{air}} = 0$ m, and an anomalous snow accumulation with $\Delta z_{\mathrm{ice}} = 0.1$ m, $\Delta z_{\mathrm{air}} = 0.2$ m. Together, the two phenomena would result in $\Delta z_{\mathrm{ice}} = -0.2$ m, $\Delta z_{\mathrm{air}} = +0.2$ m and $\Delta z = 0$ so that an apparent derived density associated with the mass and volume changes would be infinite.

RA is sensitive to Δz while GRACE is sensitive to Δz_{ice}. While Δz and Δz_{ice} are equal for pure ice dynamic effects, they are different in the presence of changes in the firn structure such as induced by SMB variations and compaction. Already for this reason, differences between ENVISAT RA height changes and GRACE ice-equivalent height changes are to be expected. Perfect knowledge of both Δz and Δz_{ice} would allow to perfectly quantify Δz_{ice} and Δz_{air}. However, the two geodetic techniques are burdened by their various specific limitations. Next, we discuss their implications for an ENVISAT RA–GRACE comparison.

Imperfections of the GIA correction induce errors in the linear trends of Δz_{ice} from GRACE and of Δz from ENVISAT. Due to the density contrast between solid Earth and ice, the effect is about four times larger for the GRACE trends than for ENVISAT RA trends (e.g. Horwath 2007, fig. 2.6 therein).

Furthermore, limitations of ENVISAT RA spatial coverage and sampling (see Section 1 and see Fig. 2b for an illustration) have an impact on spatially integrated (or filtered) ENVISAT RA changes. The impact depends on the geographic characteristics of the signal in question. For spatially coherent signals, such as related to mesoscale or larger-scale atmospheric processes, a lack of coverage is likely to just dampen the signal amplitude. For submesoscale signals, the effects of sampling limitations are prone to be more complex. Submesoscale atmospheric signals are smaller scale in the time domain (King & Turner 1997). Therefore, using lowpass filtered time-series as a representation of interannual variations allows for some mitigation of sampling issues for these signals.

The errors of both the ENVISAT RA and GRACE data products and our incomplete knowledge of the temporal and spatial covariances of these errors complicate the interpretation of ENVISAT RA–GRACE comparisons. The comparison of the independent results from ENVISAT RA and GRACE will be useful to set limits to the errors of both techniques.

The spatial sensitivity of GRACE is limited to a resolution of a few hundred kilometres. In Section 2.3 we have explained the spatial filter inherent to our GRACE results and how we impose the same filter to the ENVISAT RA maps to make the spatial resolutions compatible. Obviously, this filtering of ENVISAT RA concerns both Δz_{ice} and Δz_{air}. It corrupts our ability to perfectly isolate different ice sheet processes with different ratios between Δz_{ice} and Δz and with different spatial patterns.

To summarize, GRACE provides time-series of maps of $\Delta\tilde{z}_{\mathrm{ice}}(t)$, where the tilde is to denote the spatial filtering inherent to the GRACE solutions. ENVISAT RA provides time-series of maps of $\Delta z(t)$, which may be converted to GRACE-like filtered maps $\Delta\tilde{z}(t)$. Spatial integration of $\Delta\tilde{z}_{\mathrm{ice}}(t)$ from GRACE and $\Delta z(t)$ from RA provides mass and volume changes, respectively. Both the ENVISAT

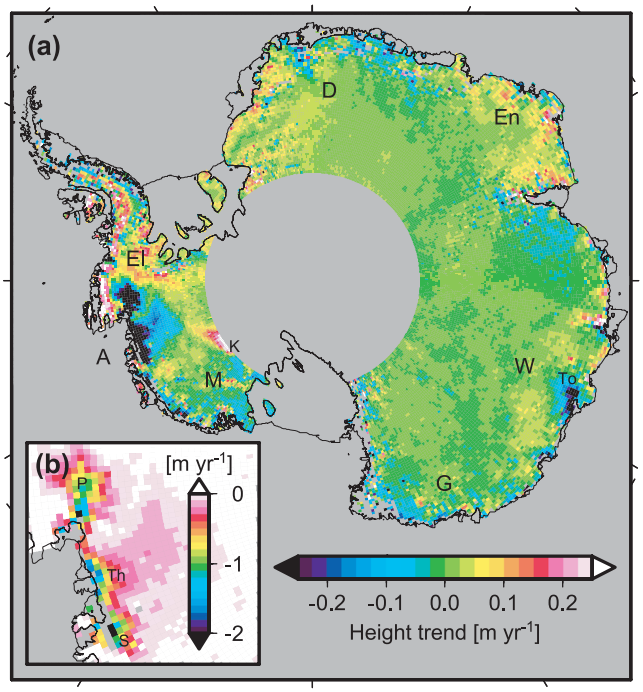

Figure 2. (a) Linear trends from ENVISAT radar altimetry ice sheet thickness variations $\Delta z(t)$ over the period 2002 October–2009 August, after GIA correction. (b) Same data shown for the Amundsen Sea Sector with a different colour scale. Geographic locations indicated by letters are as follows: A, Amundsen Sea; D, Dronning Maud Land; El, Ellsworth Land; En, Enderby Land; G, George V Land; K, Kamb Ice Stream; M, Marie Byrd Land; P, Pine Island Glacier; S, Smith, Haines, Pope and Kohler Glaciers; Th, Thwaites Glacier; To, Totten Glacier; W, Wilkes Land.

RA and GRACE results are subject to the discussed pertinent limitations.

Given these limitations, our task is to assess whether both techniques reliably reflect processes of ice sheet variation and are not dominated by errors. This is a pre-requisite of further progress in using ENVISAT RA and GRACE for describing and quantifying the different processes of ice sheet change, notably of interannual variations. Our primary approach is a qualitative comparison of patterns, both in the spatial and temporal domain. Similarity of temporal patterns is reflected by the correlation of time-series. Note that even theoretically a perfect correlation between $\Delta\tilde{z}(t)$ from ENVISAT RA and $\Delta\tilde{z}_{\rm ice}(t)$ from GRACE is not expected due to the superposition of processes with different relations between the two signals. Nonetheless, high correlation between the ENVISAT RA and GRACE time-series can be taken as an evidence of a common geophysical origin of the two results in the considered temporal and spatial scale.

3 RESULTS AND DISCUSSION

3.1 Linear trends

The linear trends of ENVISAT RA ice sheet thickness changes $\Delta z(t)$ ($0.75^\circ \times 0.2^\circ$ grid) are shown in Fig. 2. At a first glance, known trends caused by rapidly evolving ice dynamics (e.g. Davis *et al.* 2005; Zwally *et al.* 2005; Wingham *et al.* 2006; Rignot *et al.* 2008; Pritchard *et al.* 2009) may be recognized, such as strong height decreases in the Amundsen Sea Sector, an increase at Kamb Ice Stream (West Antarctica) and a decrease at Totten Glacier (East Antarctica).

Application of the GRACE-like filter to the ENVISAT RA data provides the trends of $\Delta\tilde{z}(t)$ shown in Fig. 3(a) which are compared to the linear trends of GRACE surface mass variations $\Delta\tilde{z}_{\rm ice}(t)$ shown in Fig. 3(b). With the exception of the Antarctic Peninsula with virtually no ENVISAT RA coverage, both maps agree well in their qualitative features, not only for West Antarctica but also for the alternating positive and negative trends along the East Antarctic coast.

The difference between both maps is shown in Fig. 3(c). If the observations and their processing (including corrections and filtering) had no errors and if the ENVISAT RA coverage were complete, then these differences would reflect the changes in air content of the firn. However, a large part of those differences is most plausibly explained by ENVISAT RA coverage and sampling limitations. This is obvious for the tip of the Antarctic Peninsula as well as for Kamb Ice Stream (at the polar gap limit, *cf.* Fig. 2) but also for the outlet

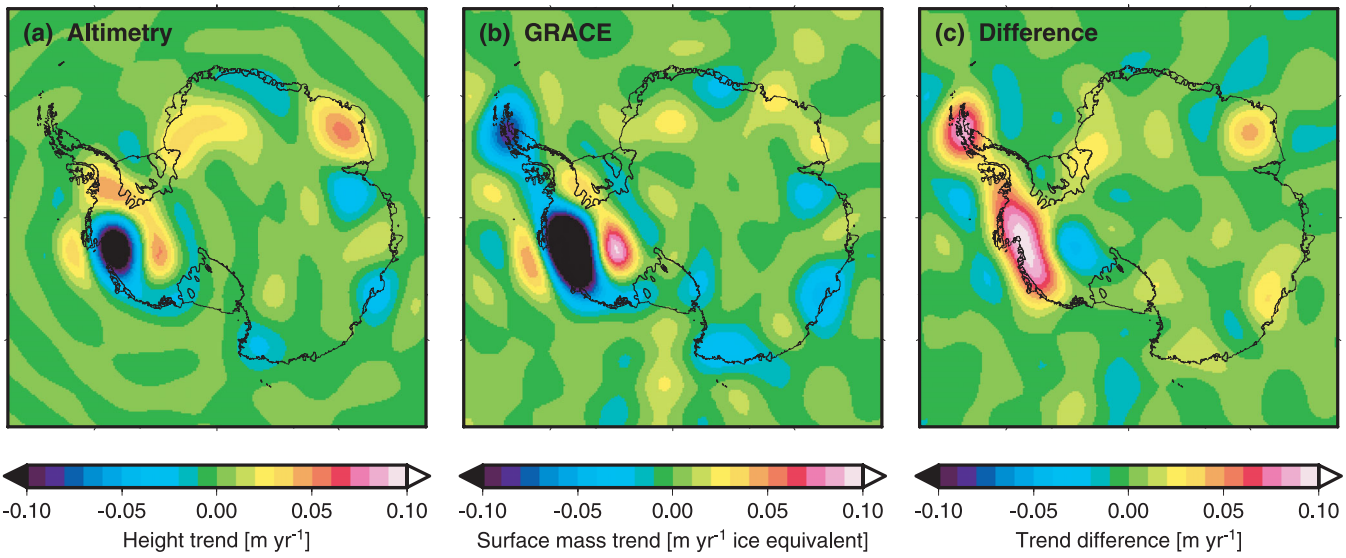

Figure 3. Linear trends of (a) the GRACE-like filtered ENVISAT RA variations $\Delta\tilde{z}(t)$ and (b) the GRACE surface mass variations $\Delta\tilde{z}_{\rm ice}(t)$. (c) Difference between the trends shown in subplots (a) and (b). GIA corrections are applied.

glaciers in the Amundsen Sea Sector where the spatial structure of ENVISAT RA trends (Fig. 2b) and previous evidence (Shepherd *et al.* 2001; Wingham *et al.* 2009) show that changes culminate at the coast. There, the ENVISAT RA data set contains a few pixels with no values (see Fig. 2b), leaving a grounded area of about 7500 km^2 uncovered. In addition, the values for other pixels might not be fully representative because the actual altimetric footprint is shifted upslope with respect to the nadir point (*cf.* Roemer *et al.* 2007; Thomas *et al.* 2008) while dynamically induced ice losses tend to be larger at lower elevations.

3.2 Interannual variations

For a detailed presentation of time-series, we selected 12 positions (circles in the map inset of Fig. 4) guided by prominent features in the trends of ENVISAT RA and GRACE and in their interannual variability. For those positions, Fig. 4(a) shows the interannual variations (as defined in Section 2.5) and Fig. 4(b) shows the linear plus interannual variations, according to GRACE-like filtered ENVISAT RA [$\Delta\tilde{z}(t)$] and GRACE [$\Delta\tilde{z}_{\rm ice}(t)$]. Frame (a) also shows the unsmoothed 10-daily time-series. The figure illustrates that beyond the linear trends, pronounced interannual variations exist. At most positions, these interannual variations are well correlated between ENVISAT RA and GRACE. Their temporal patterns vary between the subregions of the continent. For example, around 2005/2006 the curves show a pronounced minimum at position 1 (Western Dronning Maud Land) and an equally pronounced maximum at position 3 (Enderby Land).

For a more comprehensive perspective, Fig. 5 (colour code) maps the correlation between the ENVISAT RA and GRACE interannual variations over the area of ENVISAT RA coverage. In addition, contour lines display the variability of those variations. We conclude that in regions where the interannual variations of ENVISAT RA and GRACE are largest, they are well correlated, with correlation coefficients typically in the order of 0.8. (See Section 3.5 for some discussion on the negative correlation in the East Antarctic interior.)

Fig. 6 shows maps of the interannual changes from year to year. More precisely, curves analogous to the smooth curves in Fig. 4(a) were computed over a grid and the differences between the 2005.0 and 2004.0 values were mapped in subframes (a) and (f) for ENVISAT RA and GRACE, respectively, to represent the changes during the calendar year 2004. The changes over the subsequent years are represented analogously in the next subplots. While the amplitudes partly differ between the two techniques, a qualitative agreement of patterns can be observed for almost all features. Further discussion will be provided in Section 3.5.

3.3 Synthesis of high-resolution ENVISAT RA and GRACE

The consistency between ENVISAT RA and GRACE linear and interannual variations gives confidence in both independent techniques. Hence, we can approach a synthesis where GRACE provides the mass changes at large spatial scales and ENVISAT RA provides the associated high-resolution spatial patterns of height change aiding to resolve the geophysical nature of the variations.

Fig. 7 shows the year-to-year ENVISAT RA interannual changes analogous to Figs 6(a)–(e) but computed for the high-resolution grids. The depicted variations include those due to rapidly changing ice dynamics. For example, the dynamically induced acceleration of Pine Island Glacier (e.g. Rignot *et al.* 2008) is manifest

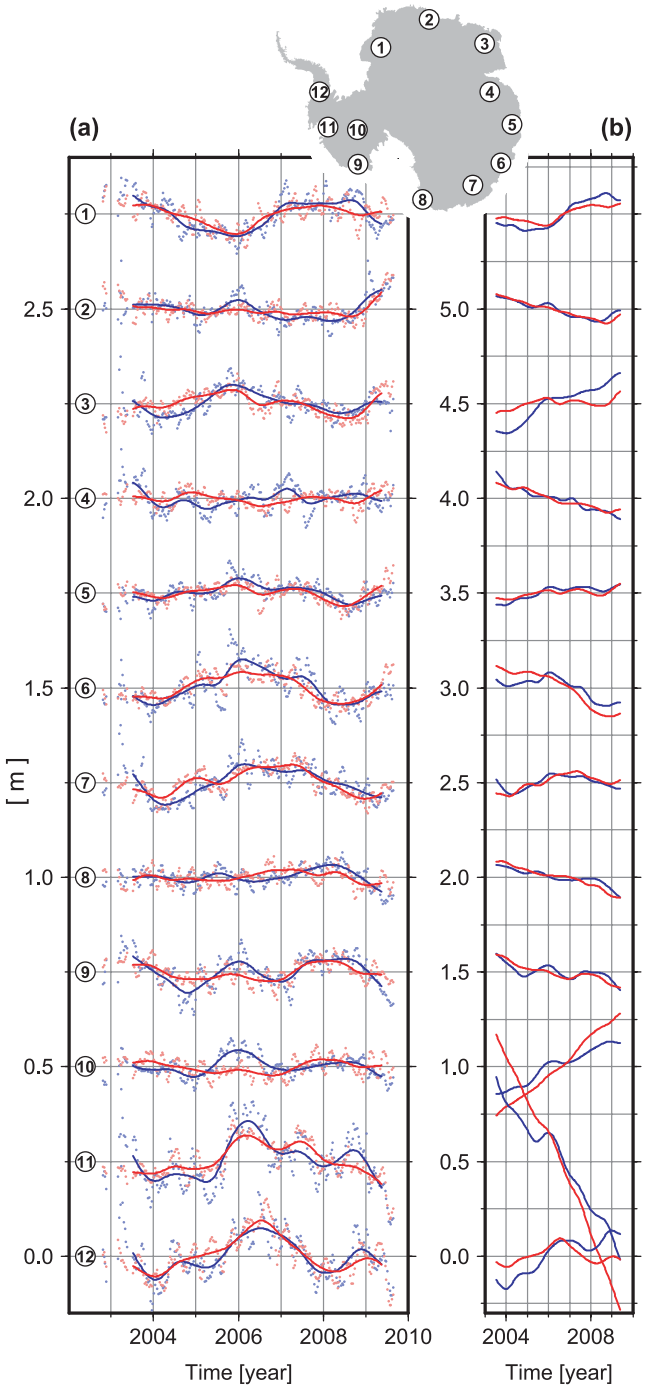

Figure 4. Comparison of time-series of GRACE-like filtered ENVISAT RA ice sheet thickness variations $\Delta\tilde{z}(t)$ (blue) versus GRACE surface mass variations $\Delta\tilde{z}_{\rm ice}(t)$ (red) at 12 positions shown in the map inset. Smooth curves in subplots (a) and (b) show the interannual and, respectively, the linear plus interannual variations. Note the different scales. Dots in subplot (a) additionally show the 10-daily unsmoothed non-linear, non-seasonal signals. Ordinate levels are arbitrarily shifted for readability.

from the relative height increase during 2004 and 2005 and the relative decrease during 2007 and 2008. As it has to be expected for dynamically induced changes, they are spatially correlated to the glacier flow pattern (*cf.* Rignot *et al.* 2008). Other features do not appear to be correlated to patterns of fast flow. Instead, they extend

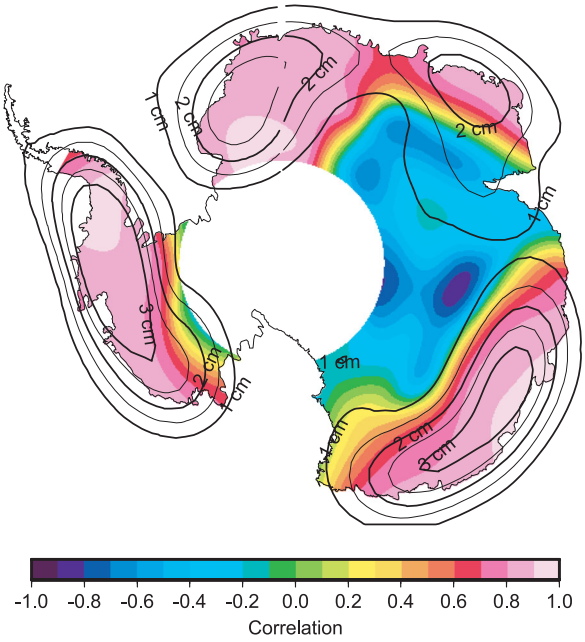

Figure 5. Colour-coded map: Correlation between the interannual variations of GRACE-like filtered ENVISAT RA [$\Delta\tilde{z}(t)$] and GRACE [$\Delta\tilde{z}_{\mathrm{ice}}(t)$]. Superposed contour lines with labels: interannual variability of ENVISAT RA and GRACE (arithmetic mean of the rms values of ENVISAT RA and GRACE). The calculations are based on time-series analogous to the smooth curves in Fig. 4(a).

rather coherently over coastal sectors of hundreds of kilometres and towards the ice sheet interior. For these patterns, SMB phenomena are a more likely cause than ice flow dynamics. Examples for such features are the relative increases in Enderby Land during 2004 and 2005, in West Antarctica and in Wilkes Land during 2005 and in Western Dronning Maud Land during 2006, and part of the decrease in George V Land during 2008 (maybe apart from the extrema near the Mertz and Ninnis Glacier tongues).

For a further exploration of interannual phenomena in the ENVISAT RA and GRACE data, an exemplary case study is conducted in the next section.

3.4 Resolving an accumulation event

For this case study, we choose the most prominent interannual feature visible in Fig. 6, namely the 2005 positive change in West Antarctica. The region of this feature is the region of largest mass changes due to rapidly changing ice dynamics, but it is also a main accumulation region of the ice sheet (James & Ivins 1995; van de Berg *et al.* 2006). Already from the timescale of 1 yr, SMB effects appear as a more likely origin of this feature than ice dynamic changes (*cf.* Joughin *et al.* 2010).

Fig. 8(a) shows the non-seasonal variations of GRACE-like filtered ENVISAT RA and GRACE at Position 11 (*cf.* map inset of Fig. 4), which is near the centre of the 2005 feature. Note, again, that due to the filtering which is inherent to the GRACE solutions and which has been imposed to the ENVISAT RA grids, the curves represent the temporal behaviour of a particular, 500 km scale, weighted spatial average of the actual variations. The curves reveal an abrupt jump-like event in 2005 September/October. We quantify the jump in a way illustrated by the black straight lines in the figure: We extract the 1-yr sections before and after the event (before August 22 and after November 10, respectively) and fit a seven-parameter function where the parameters (common to both sections) are a constant, a linear trend, annual and semi-annual cosine and sine amplitudes, and an offset between the two sections. The offset is regarded as the jump magnitude. We may apply the same operation to the time-series of GRACE-like filtered or unfiltered ENVISAT RA and GRACE at any position and, in this way, produce maps of the event magnitude. The results are shown in Fig. 9. The high-resolution ENVISAT RA map (subplots a and b) shows that the spatial pattern is not concentrated to the fast outlet glaciers. In particular, it is not pronounced in the lower reaches of Pine Island Glacier. Instead, the pattern seems related to northward slopes (leftward in Fig. 9b) and it extends far inland. These

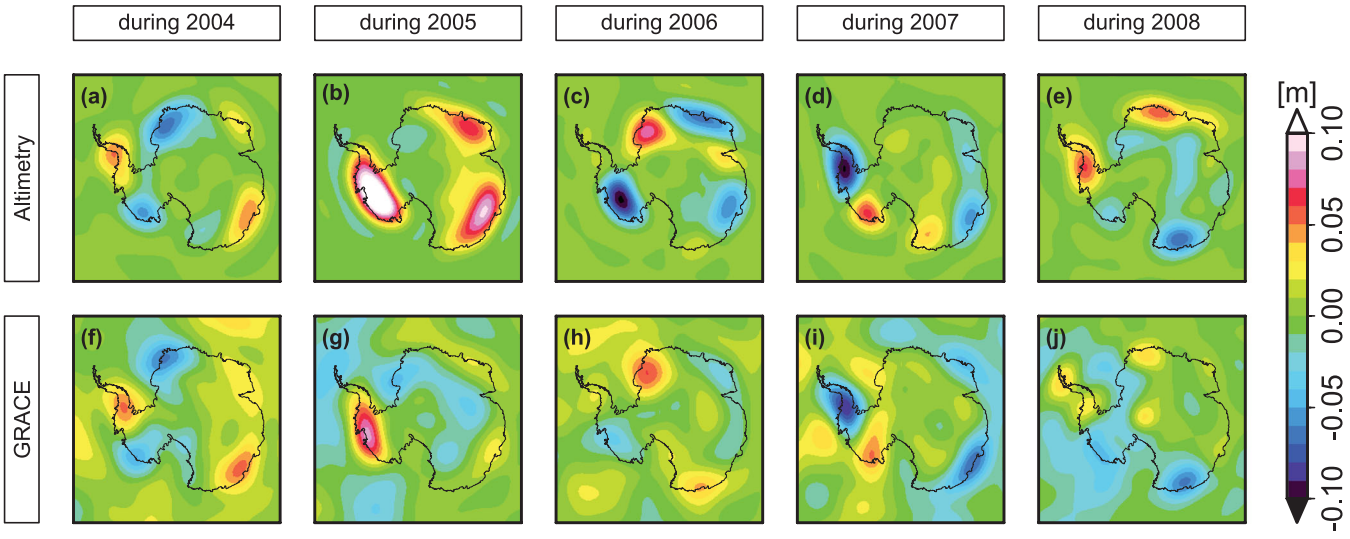

Figure 6. Year-to-year interannual changes of (top) GRACE-like filtered ENVISAT RA [$\Delta\tilde{z}(t)$] and (bottom) GRACE [$\Delta\tilde{z}_{\mathrm{ice}}(t)$]. Subplots (a) and (f) show differences between 2005 January 1 and 2004 January 1, that is, the change during the year 2004. Respective changes for the subsequent years are shown in the other subplots. The differences are based on time-series that are low-pass filtered as the smooth curves in Fig. 4(a). That is, the adopted state at 2005 January 1, for example, actually corresponds to a weighted mean with a Gaussian weight function with a two-sigma width of 0.5 yr. Linear changes are not included.

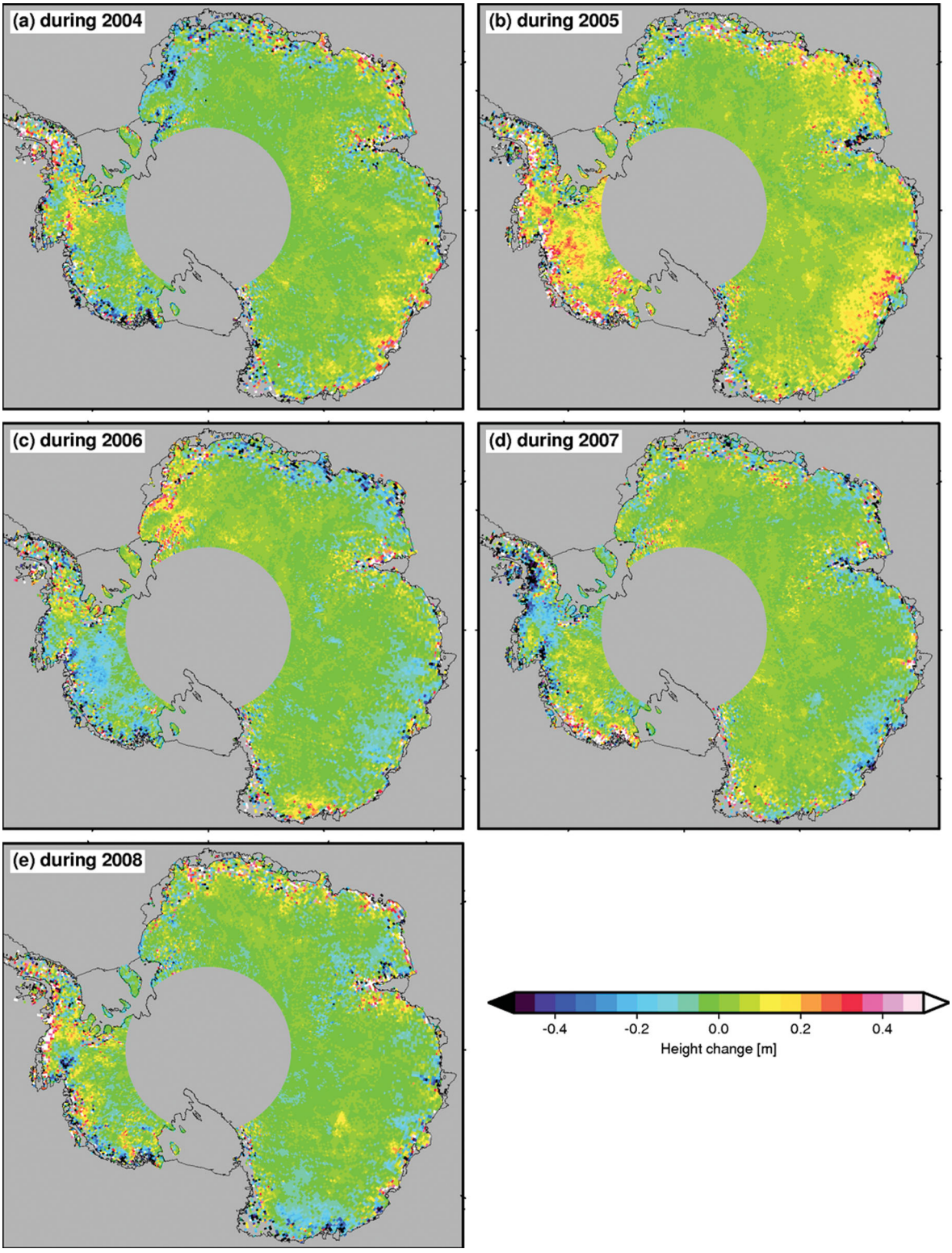

Figure 7. Year-to-year interannual variations of ENVISAT RA ice sheet thickness $\Delta z(t)$. The maps are analogous to Figs 6(a)–(e), but for the high-resolution grids. As in Fig. 6 the linear trend is not included.

characteristics strongly suggest that the jump reflects an accumulation event.

Fig. 8(b) shows the time-series of total ENVISAT RA volume effects and GRACE mass effects integrated over West Antarctica (without the Antarctic Peninsula). The respective total magnitudes of the 2005 event are $209 \pm 46\,\mathrm{km}^3$ and 82 ± 31 Gt. The cited errors are formal one-sigma errors. For their calculation we accounted for the fact that the 10-daily values represent overlapping 30-/35-d averages, which are therefore correlated. The estimated density of the accumulated snow is, consequently, 82 Gt per $209\,\mathrm{km}^3 = 394\,\mathrm{kg\,m}^{-3}$.

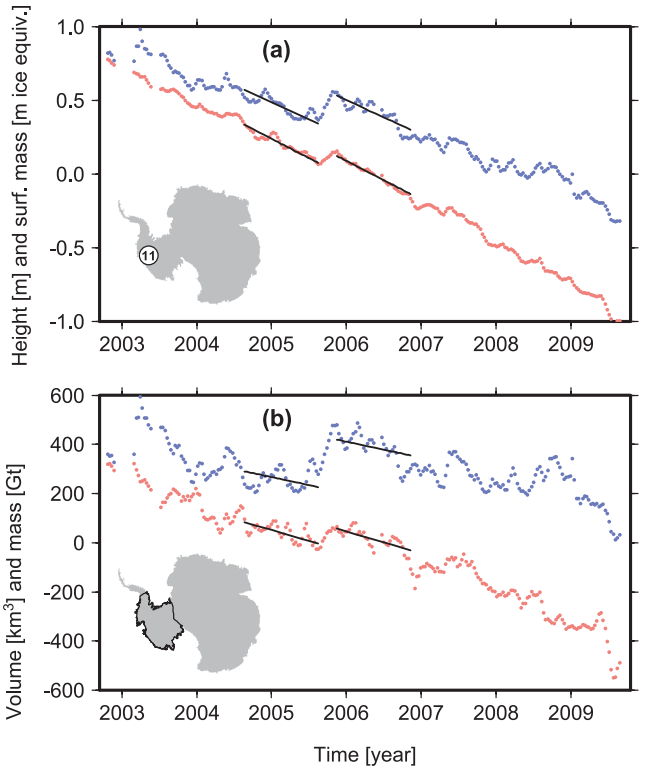

Figure 8. (a) Non-seasonal GRACE-like filtered ENVISAT RA height variations $\Delta\tilde{z}(t)$ and GRACE surface mass variations $\Delta\tilde{z}_{\mathrm{ice}}(t)$ (blue and red, respectively) at Position 11 (see map inset). (b) Integrated non-seasonal ENVISAT RA volume changes and GRACE mass changes (blue and red) over West Antarctica (without the Antarctic Peninsula; see map inset). Ordinate levels are arbitrarily shifted for readability. Black lines illustrate the estimation of the 2005 jump magnitude. It is estimated as the offset between two straight lines of equal trend adjusted together with common annual and semi-annual sinusoids to 1-yr sections before and after the event.

The formal one-sigma intervals of the mass and volume magnitudes allow for a rather large range of densities between 201 and 696 kg m^{-3}, even though these error estimates do not cover all error sources.

3.5 Discussion

Our quantification of the 2005 accumulation event (Section 3.4) adopted equal trends before and after the event as a reference. This simple choice is guided by the demand for robustness in the presence of errors. Generally, the definition of a reference to which interannual variations should refer is not obvious and may affect interpretation. Our overall, pragmatic approach (e.g. for Figs 4a and 6; *cf.* Section 2.5) has been to refer interannual variations to a linear function adjusted to the entire observation period. This likely absorbs linear effects of interannual SMB variations. Conversely, this approach retains non-linear, possibly long-term effects of changing ice dynamics in our representation of interannual variations. The Amundsen Sea Basin is an illustrative example. Given the evidence for accelerated dynamically induced ice loss at Pine Island Glacier (e.g. Rignot *et al.* 2008), the non-linear variations depicted for Position 11 in Fig. 4 are a superposition of ice dynamics and SMB effects. Therefore it would be premature to interpret trend differences before and after the 2005 accumulation event in

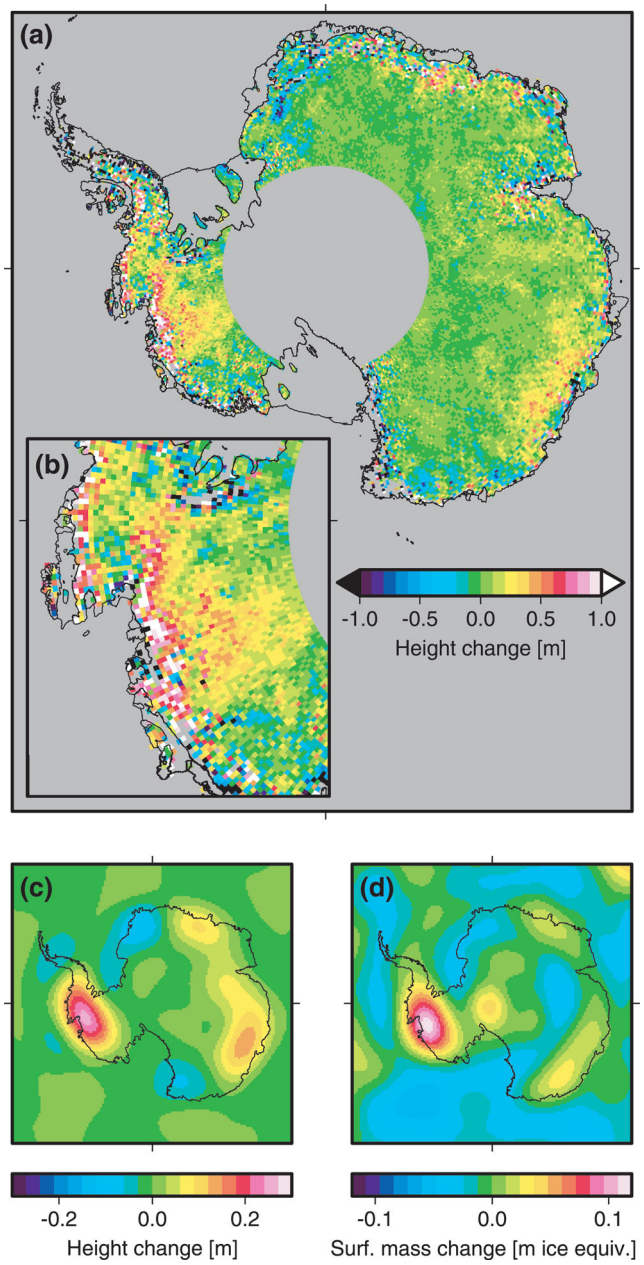

Figure 9. Magnitude of the 2005 event adjusted to (a) the high resolution ENVISAT RA variations $\Delta z(t)$; (b) same as (a), magnified for West Antarctica; (c) the GRACE-like filtered ENVISAT RA variations $\Delta\tilde{z}(t)$; (d) the GRACE surface mass variations $\Delta\tilde{z}_{\mathrm{ice}}(t)$.

terms of firn-related processes such as post-event wind erosion or excess compaction.

The task of separating the interannual signal is further complicated by the challenge of error assessment for the ENVISAT RA and GRACE data sets. As mentioned earlier, ENVISAT RA uncertainties include coverage and representativeness issues which may change with time. Interannual GRACE error issues are, for example, manifest in the occurrence of the 2005 September/October event in Wilkes Land, East Antarctica. The event shows up in the ENVISAT RA time-series of the region (curves 5–7 in Fig. 4a and Figs 9a and c). The associated GRACE pattern in Fig. 9(d) has a similar contrast between coastal and interior areas as the ENVISAT RA pattern in Fig. 9(c). However, GRACE shows a negative signal in the ice sheet

interior accompanying the positive signal near the coast. The inland change is geophysically doubtful just as the small, pronounced positive feature at the South Pole is. We may suspect errors in the GRACE solutions. Indeed, we have found that the systematic errors in the GRACE solutions identified by Horwath *et al.* (2011) are a least partly responsible for the dubious GRACE feature. Note, incidentally, that the suspect GRACE feature is a major reason why correlations shown in Fig. 5 are negative in parts of interior East Antarctica.

It is appealing, yet beyond the scope of this paper, to perform detailed comparisons of the present geodetic results with atmospheric modelling results. For the Amundsen Sea Sector (as well as for the Antarctic Peninsula), Sasgen *et al.* (2010a) have reported agreement between ECMWF (European Centre for Medium-Range Weather Forecasts) variations of precipitation minus evaporation and GRACE-derived mass variations. Their Fig. 4(b) shows that the ECMWF model contains an excess accumulation in the second half of 2005 which, from the figure, we roughly quantify to be in the order of 60 Gt. This result refers to an integration over a subregion of West Antarctica while our estimate of 82 Gt refers to entire West Antarctica. The 2005 excess accumulation that we diagnosed from geodetic data is hence supported by ECMWF atmospheric modelling.

4 CONCLUSIONS

Even though ENVISAT RA and GRACE satellite gravimetry have their specific limitations and different relative sensitivities to ice flow- and SMB-related processes, the two techniques show consistent patterns of ice sheet changes not only for linear trends but also for interannual variations. This consistency establishes mutually corroborative evidence for the ENVISAT RA and GRACE time-series. Both have quite robust power to perform investigations on interannual timescale mass changes in Antarctica.

The combination of both techniques adds value to either observation and aids their interpretation. Specifically, we were able do describe and quantify an event of excess accumulation in West Antarctica in 2005 September/October. We also discussed the challenges related to the identification of interannual anomalies (also in the presence of non-linear long-term changes due to ice dynamics), their interpretation and quantification.

We expect benefits from a combination with regional atmospheric modelling. The ensemble of satellite altimetry and satellite gravimetry data may be used to validate modelled SMB variations which might lead to eventual improvements in the SMB modelling and contribute to reduce present uncertainties on Antarctic SMB.

As a major limitation of conventional RA, the lack of coverage at ice sheet margins will be largely overcome by CryoSat-2 (launched in 2010 April) and the future Sentinel-3 mission. A combination with the complementary ICESat laser altimetry will be attractive as well. Satellite altimetry and gravimetry missions must continue and combination methods must be further developed for the aim of better resolving the nature of variations, enhancing the accuracies, and linking past, present and future changes.

ACKNOWLEDGMENTS

MH was funded by a research fellowship of the Deutsche Forschungsgemeinschaft (DFG), grant number Ho 4232/1-1. Support to this study was also granted by the Agence Nationale de la Recherche (ANR) in the framework of the VANISH project. The ENVISAT data were acquired through the LEGOS CTOH Altimetry database at GDR level and processed within the OSCAR project. The GRACE solutions were acquired through the CNES/GRGS database. Atmospheric delay tests were made using ECMWF ERA-INTERIM data. The Global Ionosphere model TEC Maps used to compute the ionospheric delay were downloaded from the corresponding JPL website. We acknowledge the comments by three anonymous reviewers and the editor I. Velicogna, which helped to improve the manuscript.

REFERENCES

Alley, R.B., Clark, P.U., Huybrechts, P. & Joughin, I., 2005. Ice-sheet and sea-level changes, *Science,* **310,** 456–460.

Alley, R.B., Spencer, K. & Anandakrishnan, S., 2007. Ice-sheet mass balance: assessment, attribution and prognosis, *Ann. Glaciol.,* **46,** 1–7.

Allison, I., Alley, R., Fricker, H., Thomas, R. & Warner, R., 2009. Ice sheet mass balance and sea level, *Antarct. Sci.,* **21**(5), 413–426, doi:10.1017/S0954102009990137.

Arthern, R. & Hindmarsh, R., 2003. Optimal estimation of changes in the mass of ice sheets, *J. geophys. Res.,* **108**(F1), 6007, doi:10.1029/2003JF000021.

Arthern, R.J., Wingham, D.J. & Ridout, A.J., 2002. Controls on ERS altimeter measurements over ice sheets: footprint-scale topography, backscatter fluctuations, and the dependence of microwave penetration depth upon satellite orientation, *J. geophys. Res.,* **106**(D24), 33471–33484, doi:10.1029/2001JD000498.

van de Berg, W.J., van den Broeke, M.R., Reijmer, C. & van Meijgaard, E., 2006. Reassessment of the Antarctic surface mass balance using calibrated output of a regional atmospheric climate model, *J. geophys. Res.,* **41**(1), 97–104.

Berrisford, P., Dee, D., Fielding, K., Fuentes, M., Kallberg, P., Kobayashi, S. & Uppala, S., 2009. The ERA-interim archive, Tech. Rep., ECMWF ERA Report Series.

Bindschadler, R., 2006. The environment and evolution of the West Antarctic ice sheet: setting the stage, *Phil. Trans. R. Soc. A,* **364**(1844), 1583–1605, doi:10.1098/rsta.2006.1790.

Blarel, F., 2010. Investigations on the ENVISAT RA2 Dry Troposphere correction for ice sheets, ESA ENVISAT RA2 Quality Working Group Technical Report.

van den Broeke, M.R., Bamber, J., Lenaerts, J. & Rignot, E., 2011. Ice sheets and sea level: thinking outside the box, *Surv. Geophys.,* **32**(4–5), 495–505, doi:10.1007/s10712-011-9137-z.

Bruinsma, S., Lemoine, J.-M., Biancale, R. & Valès, N., 2010. CNES/GRGS 10-day gravity field models (release 2) and their evaluation, *Adv. Space Res.,* **45,** 587–601, doi:10.1016/j.asr.2009.10.012.

Chen, J.L., Wilson, C.R., Tapley, B.D., Blankenship, B. & Young, D., 2008. Antarctic regional ice loss rates from GRACE, *Earth planet. Sci. Lett.,* **266,** 140–148, doi:10.1016/j.epsl.2007.10.057.

Davis, C.H., Li, Y., McConnell, J.R., Frey, M.M. & Hanna, E., 2005. Snowfall-driven growth in East Antarctic ice sheet mitigates recent sea-level rise, *Science,* **308**(5730), 1898–1901, doi:10.1126/science.1110662.

Eisen, O. et al., 2008. Ground-based measurements of spatial and temporal variability of snow accumulation in East Antarctica, *Rev. Geophys.,* **46**(RG2001), doi:10.1029/2006RG000218.

ESA, 2007. ENVISAT RA2/MWR Product Handbook, Issue 2.2, Tech. Rep., European Space Agency.

Greuell, W. & Genthon, C., 2004. Modelling land-ice surface mass balance, in *Mass Balance of the Cryosphere: Observations and Modelling of Contemporary and Future Changes,* pp. 117–168, eds Bamber, J. & Payne, A., Cambridge University Press, Cambridge.

Gunter, B. *et al.*, 2009. A comparison of coincident GRACE and ICESat data over Antarctica, *J. Geod.,* **83**(11), 1051–1060, doi:10.1007/s00190-009-0323-4.

Heiskanen, W.A. & Moritz, H., 1967. *Physical Geodesy,* W.H. Freeman and Co., San Francisco.

Helsen, M.M., van den Broeke, M.R., van de Wal, R.S.W., van de Berg, W.J., van Meijgaard, E., Davis, C.H., Li, Y. & Goodwin, I., 2008. Elevation

changes in Antarctica mainly determined by accumulation variability, *Science,* **320**(5883), 1626–1629, doi:10.1126/science.1153894.

Horwath, M., 2007. Determining geophysical mass signals with gravity field missions: an analysis of the current status with regard to Antarctica, *Ph.D. thesis*, Technische Universität Dresden, Fakultät Forst-, Geo- und Hydrowissenschaften, http://nbn-resolving.de/urn:nbn:de:bsz:14-ds-1203684703310-42192 (in German).

Horwath, M. & Dietrich, R., 2006. Errors of regional mass variations inferred from GRACE monthly solutions, *Geophys. Res. Lett.,* **33,** L07502, doi:10.1029/2005GL025550.

Horwath, M. & Dietrich, R., 2009. Signal and error in mass change inferences from GRACE: the case of Antarctica, *Geophys. J. Int.,* **177**(3), 849–864, doi:10.1111/j.1365-246X.2009.04139.x.

Horwath, M., Dietrich, R., Bäßler, M., Nixdorf, U., Steinhage, D., Fritzsche, D., Damm, V. & Reitmayr, G., 2006. Nivlisen, an Antarctic ice shelf in Dronning Maud Land: geodetic-glaciological results from a combined analysis of ice thickness, ice surface height and ice flow observations, *J. Glaciol.,* **52**(176), 17–30.

Horwath, M., Lemoine, J.-M., Biancale, R. & Bourgogne, S., 2011. Improved GRACE science results after adjustment of geometric biases in the Level-1B K-band ranging data, *J. Geod.,* **85,** 23–38, doi:10.1007/s00190-010-0414-2.

Iijima, B.A., Harris, I.L., Lindqwister, C.M.H.U.J., Mannucci, A.J., Pi, X., Reyes, M.J., Sparks, L.C. & Wilson, B.D., 1999. Automated daily process for global ionospheric total electron content maps and satellite ocean altimeter ionospheric calibration based on Global Positioning System data, *J. Atmos. Sol.-Terr. Phys.,* **61**(16), 1205–1218.

Ivins, E.R. & James, T.J., 2005. Antarctic glacial isostatic adjustment: a new assessment, *Antarct. Sci.,* **17**(4), 541–553.

James, T.J. & Ivins, E., 1995. Present-day Antarctic ice mass changes and crustal motion, *Geophys. Res. Lett.,* **22**(8), 973–976.

Joughin, I., Smith, B.E. & Holland, D.M., 2010. Sensitivity of 21st century sea level to ocean-induced thinning of Pine Island Glacier, Antarctica, *Geophys. Res. Lett.,* **37**(L20502), doi:10.1029/2010GL044819.

King, J.C. & Turner, J., 1997. *Antarctic Meteorology and Climatology,* Cambridge University Press, Cambridge.

Klokočník, J., Wagner, C.A., McAdoo, D., Kostelecký, J., Bezděk, A. & Novák, P., 2008. Variations in the accuracy of gravity recovery due to ground track variability: GRACE, CHAMP, and GOCE, *J. Geod.,* **82**(12), 917–927, doi:10.1007/s00190-008-0222-0.

Kusche, J., 2007. Approximate decorrelation and non-isotropic smoothing of time-variable GRACE-type gravity field models, *J. Geod.,* **81**(11), 733–749, doi:10.1007/s00190-007-0143-3.

Lacroix, P., Legrésy, B., Rémy, F. & Blarel, F., 2009. Rapid change of the snow surface properties at Vostok, East Antarctica, revealed by altimetry, *Remote Sens. Environ.,* **113,** 2633–2641, doi:10.1016/j.rse.2009.07.019.

Legrésy, B. & Rémy, F., 1997. Altimetric observations of surface characteristics of the Antarctic ice sheet, *J. Glaciol.,* **43**(144), 265–275.

Legrésy, B. & Rémy, F., 1998. Using the temporal variability of satellite radar altimetry observations to map surface properties of the Antarctic ice sheet, *J. Glaciol.,* **44**(147), 197–206.

Legrésy, B., Papa, F., Rémy, F., Vinay, G., van den Bosch, M. & Zanife, O.-Z., 2005. ENVISAT radar altimeter measurements over continental surfaces and ice caps using the ICE-2 retracking algorithm, *Remote Sens. Environ.,* **95,** 150–163.

Legrésy, B., Rémy, F. & Blarel, F., 2006. Along track repeat altimetry for ice sheets and continental surface studies, in *Proceedings of Symposium on 15 Years of Progress in Radar Altimetry,* Venice, Italy, 13–18 March 2006, Vol. 614 of ESA-SP, p. 181, European Space Agency Publication Division, Noordwijk, The Netherlands.

Lemoine, J.-M., Bruinsma, S., Loyer, S., Biancale, R., Marty, J.-C., Perosanz, F. & Balmino, G., 2007. Temporal gravity field models inferred from GRACE data, *Adv. Space Res.,* **39**(10), 1620–1629, doi:10.1016/j.asr.2007.03.062.

Ligtenberg, S. R.M., Helsen, M.M. & van den Broeke, M.R., 2011. An improved semi-empirical model for the densification of Antarctic firn, *Cryosphere,* **5,** 809–819, doi:10.5194/tc-5-809-2011.

Monaghan, A.J. & Bromwich, D.H., 2008. Advances in describing recent Antarctic climate variability, *Bull. Am. Meteorol. Soc.,* **89,** 1295–1306.

Moore, P. & King, M.A., 2008. Antarctic ice mass balance estimates from GRACE: tidal aliasing effects, *J. geophys. Res.,* **113**(F02005), doi:10.1029/2007JF000871.

Pritchard, H.D., Arthern, R.J., Vaughan, D.G. & Edwards, L.A., 2009. Extensive dynamic thinning on the margins of the Greenland and Antarctic ice sheets, *Nature,* **461,** 971–975, doi:10.1038/nature08471.

Ramillien, G., Lombard, A., Cazenave, A., Ivins, E.R., Llubes, M., Rémy, F. & Biancale, R., 2006. Interannual variations of the mass balance of the Antarctica and Greenland ice sheets from GRACE, *Global Planet. Change,* **53,** 198–208.

Rémy, F. & Parrenin, F., 2004. Snow accumulation variability and random walk: how to interpret changes of surface elevation in Antarctica, *Earth planet. Sci. Lett.,* **227**(3/4), 273–280, doi:10.1016/j.epsl.2004.09.003.

Rémy, F., Mazzega, P., Houry, S., Brossier, C. & Minster, J.F., 1989. Mapping of the topography of continental ice by inversion of satellite-altimeter data, *J. Glaciol.,* **35**(119), 98–107.

Rignot, E., Bamber, J., van den Broeke, M.R., Davis, C., Li, Y., van de Berg, W.J. & van Meijgaard, E., 2008. Recent Antarctic ice mass loss from radar interferometry and regional climate modelling, *Nat. Geosci.,* **1,** 106–110, doi:10.1038/ngeo102.

Rignot, E., Velicogna, I., van den Broeke, M., Monaghan, A. & Lenaerts, J., 2011. Acceleration of the contribution of the Greenland and Antarctic ice sheets to sea level rise, *Geophys. Res. Lett.,* **38,** L05503, doi:10.1029/2011GL046583.

Riva, R.E.M. *et al.*, 2009. Glacial Isostatic adjustment over Antarctica from combined ICESat and GRACE satellite data, *Earth planet. Sci. Lett.,* **288,** 516–523, doi:10.1016/j.epsl.2009.10.013.

Roemer, S., Legrésy, B., Horwath, M. & Dietrich, R., 2007. Refined analysis of radar altimetry data applied to the region of the subglacial Lake Vostok/Antarctica, *Remote Sens. Environ.,* **106,** 269–284, doi:10.1016/j.rse.2006.02.026.

Sasgen, I., Martinec, Z. & Fleming, K., 2007. Regional ice-mass changes and glacial-isostatic adjustment in Antarctica from GRACE, *Earth planet. Sci. Lett.,* **264,** 391–401, doi:10.1016/j.epsl.2007.09.029.

Sasgen, I., Dobslaw, H., Martinec, Z. & Thomas, M., 2010a. Satellite gravimetry observation of Antarctic snow accumulation related to ENSO, *Earth planet. Sci. Lett.,* **299**(3–4), doi:10.1016/j.epsl.2010.09.015.

Sasgen, I., Martinec, Z. & Bamber, J., 2010b. Combined GRACE and InSAR estimate of West Antarctic ice-mass loss, *J. geophys. Res.,* **115,** F04010, doi:10.1029/2009JF001543.

Schmidt, R., Flechtner, F., Meyer, U., Neumayer, K.-H., Dahle, C., König, R. & Kusche, J., 2008. Hydrological signals observed by the GRACE satellites, *Surv. Geophys.,* **29,** 319–334, doi:10.1007/s10712-008-9033-3.

Schutz, B.E., Zwally, H.J., Shuman, C.A., Hanock, D. & DiMarzio, J.P., 2005. Overview of the ICESat mission, *Geophys. Res. Lett.,* **32,** L21S01, doi:10.1029/2005GL024009.

Shepherd, A., Wingham, D., Mansley, J.A.D. & Corr, H.F.J., 2001. Inland thinning of Pine Island Glacier, West Antarctica, *Science,* **291,** 862–864.

Solomon, S., Qin, D., Manning, M., Chen, Z., Marquis, M., Averyt, K.B., Tignor, M. & Miller, H.L., 2007. *Climate Change 2007: The Physical Basis. Contribution of Working Group I to the Fourth Assessment Report of the Intergovernmental Panel on Climate Change,* Cambridge University Press, Cambridge.

Thomas, I.D. et al., 2011. Widespread low rates of Antarctic glacial isostatic adjustment revealed by GPS observations, *Geophys. Res. Lett.,* **38,** L22302, doi:10.1029/2011GL049277.

Thomas, R., Davis, C., Frederick, E., Krabill, W., Li, Y., Manizade, S. & Martin, C., 2008. A comparison of Greenland ice-sheet volume changes derived from altimetry measurements, *J. Glaciol.,* **54**(185), 203–212, doi:10.3189/002214308784886225.

Vaughan, D.G., Bamber, J.L., Giovinetto, M., Russell, J. & Cooper, P.R., 1999. Reassessment of net surface mass balance in Antarctica, *J. Clim.,* **12,** 933–946.

Velicogna, I., 2009. Increasing rates of ice mass loss from the Greenland and Antarctic ice sheets revealed by GRACE, *Geophys. Res. Lett.,* **36,** L19503, doi:10.1029/2009GL040222.

Velicogna, I. & Wahr, J., 2010. Ice sheet mass balance with GRACE: precision and limitations, in *Proceedings of GRACE Science Team Meeting,* November 11–12, 2010, Potsdam, Germany.

Wahr, J., Molenaar, M. & Bryan, F., 1998. Time variability of the Earth's gravity field: hydrological and oceanic effects and their possible detection using GRACE, *J. geophys. Res.,* **103**(B12), 30 205–30 229.

Wahr, J., Wingham, D. & Bentley, C., 2000. A method of combining ICESat and GRACE satellite data to constrain Antarctic mass balance, *J. geophys. Res.,* **105**(B7), 16 279–16 294.

Werth, S., Güntner, A., Schmidt, R. & Kusche, J., 2009. Evaluation of GRACE filter tools from a hydrological perspective, *Geophys. J. Int.,* **179,** 1499–1515 doi:10.1111/j.1365-246X.2009.04355.x.

Wingham, D.J., Ridout, A.J., Scharroo, R., Arthern, R.J. & Shum, C.K., 1998. Antarctic elevation change from 1992 to 1996, *Science,* **282,** 456–458.

Wingham, D.J., Shepherd, A., Muir, A. & Marshall, G.J., 2006. Mass balance of the Antarctic ice sheet, *Phil. Trans. R. Soc. A,* **364**(1844), 1627–1635, doi:10.1098/rsta.2006.1792.

Wingham, D.J., Wallis, D.W. & Shepherd, A., 2009. Spatial and temporal evolution of Pine Island Glacier thinning 1995-2006, *Geophys. Res. Lett.,* **36,** L17501, doi:10.1029/2009GL039126.

Zwally, H.J., Giovinetto, M.B., Li, J., Cornejo, H.G., Beckley, M.A., Brenner, A.C., Saba, J.L. & Yi, D., 2005. Mass changes of the Greenland and Antarctic ice sheets and shelves and contributions to sea-level rise: 1992-2002, *J. Glaciol.,* **51**(175), 509–527, doi:10.3189/172756505781829007.

APPENDIX A: GRACE-LIKE FILTERING OF GEOPHYSICAL SURFACE MASS SIGNALS

The 10-d gravity field solutions are generated by estimating Stokes coefficient residuals Δc_{nm} ($n = 2, \ldots, n_{\max}$; $m = -n, \ldots, n$) with respect to the background gravity field model. They represent gravity field residuals, which can be expressed in terms of the geoid height by the spherical harmonic (*SH*) expansion

$$\Delta N(\Omega) = a \sum_{nm} \Delta c_{nm} Y_{nm}(\Omega), \tag{A1}$$

where a is the semi-major axis, $\sum_{nm}$ denotes $\sum_{n=2}^{n_{\max}} \sum_{m=-n}^{n}$ and $Y_{nm}(\Omega)$ (with the spherical position Ω) are the fully normalized *SH* base functions of degree n and order $|m|$ (e.g. Heiskanen & Moritz 1967; Wahr *et al.* 1998), with positive or negative m indicating cosine or sine dependence on longitude. For any gravity field anomaly (represented by Δc_{nm}), there is an equivalent anomaly of global surface masses, $\Delta\kappa(\Omega)$ (commonly expressed in kg m^{-2} or mm w.e. height) that would induce this gravity field anomaly (Wahr *et al.* 1998). In the *SH* expansion of $\Delta\kappa(\Omega)$,

$$\Delta\kappa(\Omega) = \sum_{nm} \Delta\kappa_{nm} Y_{nm}(\Omega), \tag{A2}$$

the coefficients $\Delta\kappa_{nm}$ are

$$\Delta\kappa_{nm} = K_n \Delta c_{nm} \tag{A3}$$

with

$$K_n = \frac{2n+1}{1+k'_n} \frac{M}{4\pi a^2}, \tag{A4}$$

where k'_n are the load Love numbers and M is the Earth's mass (Wahr *et al.* 1998).

We want to elaborate how the regularization of the gravity field solution affects the equivalent surface mass changes. Let $\Delta\kappa(\Omega)$ and $\Delta\tilde{\kappa}(\Omega)$ denote surface mass residuals equivalent to an unregularized solution and a regularized solution, respectively. The relation between $\Delta\kappa(\Omega)$ and $\Delta\tilde{\kappa}(\Omega)$ can be regarded as a linear filter. Its general form in the spatial domain is given by the following integral over the unit sphere:

$$\Delta\tilde{\kappa}(\Omega) = \frac{1}{4\pi} \iint_{\Omega'} w(\Omega', \Omega) \Delta\kappa(\Omega') \mathrm{d}\Omega'. \tag{A5}$$

The kernel $w(\Omega', \Omega)$ is to be specified in the following.

With Δc_{nm} and $\Delta\tilde{c}_{nm}$ denoting the Stokes coefficient residuals from an unregularized and a regularized solution, respectively, we employ a vector notation by arranging all Δc_{nm} (and, respectively, all $\Delta\tilde{c}_{nm}$) in a column vector $\mathbf{\Delta c}$ (and, respectively, $\mathbf{\Delta\tilde{c}}$) according to the sorting order used in the normal equations. Then, the relation between both sets of coefficients is described with the filter matrix F of (1) (Kusche 2007):

$$\mathbf{\Delta\tilde{c}} = F \mathbf{\Delta c}. \tag{A6}$$

With an analogous vector notation, (A2) reads

$$\Delta\kappa(\Omega) = \boldsymbol{y}^T(\Omega) \mathbf{\Delta\kappa}, \tag{A7}$$

where $\boldsymbol{y}(\Omega)$ and $\mathbf{\Delta\kappa}$ are the vectors arranging the $Y_{nm}(\Omega)$ and the $\Delta\kappa_{nm}$, always with the same sorting order of the (n, m) pairs. Eq. (A3) can be written as

$$\mathbf{\Delta\kappa} = K \mathbf{\Delta c}, \tag{A8}$$

where K is a diagonal matrix with the appropriate, multiple entries of K_n on its diagonal. In analogy to (A7), the surface mass change equivalent to the regularized solution is

$$\Delta\tilde{\kappa}(\Omega) = \boldsymbol{y}^T(\Omega) \mathbf{\Delta\tilde{\kappa}}, \tag{A9}$$

where, by (A8) and (A6),

$$\mathbf{\Delta\tilde{\kappa}} = K \mathbf{\Delta\tilde{c}} = KF \mathbf{\Delta c} = KFK^{-1} \mathbf{\Delta\kappa}. \tag{A10}$$

Eq. (A10) is the spectral description of the filter effect on surface mass signals. It follows that

$$\Delta\tilde{\kappa}(\Omega) = \boldsymbol{y}^T(\Omega) KFK^{-1} \mathbf{\Delta\kappa}. \tag{A11}$$

The filter kernel $w(\Omega', \Omega)$ of (A5) can be expanded into a *SH* series as a function of Ω':

$$w(\Omega', \Omega) = \sum_{nm} w_{nm}(\Omega) Y_{nm}(\Omega'). \tag{A12}$$

In vector notation, the last equation reads

$$w(\Omega', \Omega) = \boldsymbol{w}^T(\Omega) \boldsymbol{y}(\Omega'), \tag{A13}$$

where $\boldsymbol{w}(\Omega)$ is the column vector of the coefficients $w_{nm}(\Omega)$. By inserting (A12) and (A2) into (A5) and by accounting for the orthogonality relations between the *SH* base functions we get

$$\Delta\tilde{\kappa}(\Omega) = \sum_{nm} w_{nm}(\Omega) \Delta\kappa_{nm} \tag{A14}$$

$$= \boldsymbol{w}^T(\Omega) \mathbf{\Delta\kappa}. \tag{A15}$$

Comparison of (A15) and (A11) reveals

$$\boldsymbol{w}^T(\Omega) = \boldsymbol{y}^T(\Omega) KFK^{-1}. \tag{A16}$$

Insertion of (A16) into (A13) finally specifies the filter kernel as

$$w(\Omega', \Omega) = \boldsymbol{y}^T(\Omega) K F K^{-1} \boldsymbol{y}(\Omega'), \tag{A17}$$

or, in a sum notation,

$$w(\Omega', \Omega) = \sum_{nm} \sum_{n'm'} F_{nm,n'm'} K_n Y_{nm}(\Omega) K_{n'}^{-1} Y_{n'm'}(\Omega'), \tag{A18}$$

where $F_{nm,n'm'}$ is the element of the filter matrix F in the row attributed to (n, m) and the column attributed to (n', m').

Note that by the presence of K and K^{-1} in (A17) the filter kernel for surface masses is different from the filter kernel for geoid heights or for other gravity field functionals. Kernels for such other functionals may be obtained by obvious modifications of the given derivation.